




Article

Peroxidase-Like Metal-Based Nanozymes: Synthesis, Catalytic Properties, and Analytical Application

Olha Demkiv^{1,2}, Nataliya Stasyuk¹, Roman Serkiz¹ , Galina Gayda^{1,*} , Marina Nisnevitch^{3,*} 
and Mykhailo Gonchar^{1,4}

¹ Institute of Cell Biology, National Academy of Sciences of Ukraine, 79005 Lviv, Ukraine; demkivo@nas.gov.ua (O.D.); stasukne@nas.gov.ua (N.S.); rserkiz@gmail.com (R.S.); gonchar@cellbiol.lviv.ua (M.G.)

² Faculty of Veterinary Hygiene, Ecology and Law, Stepan Gzhytskyi National University of Veterinary Medicine and Biotechnologies, 79000 Lviv, Ukraine

³ Department of Chemical Engineering, Ariel University, Kyriat-ha-Mada, Ariel 4070000, Israel

⁴ Department of Biology and Chemistry, Drohobych Ivan Franko State Pedagogical University, 82100 Drohobych, Ukraine

* Correspondence: galina.gayda@gmail.com or galina.gayda@nas.gov.ua (G.G.); marinan@ariel.ac.il (M.N.); Tel.: +380-226-2144 (G.G.); +972-3914-3042 (M.N.)

Abstract: Nanozymes (NZs) are nanostructured artificial enzymes that mimic catalytic properties of natural enzymes. The NZs have essential advantages over natural enzymes, namely low preparation costs, stability, high surface area, self-assembling capability, size and composition-dependent activities, broad possibility for modification, and biocompatibility. NZs have wide potential practical applications as catalysts in biosensorics, fuel-cell technology, environmental biotechnology, and medicine. Most known NZs are mimetics of oxidoreductases or hydrolases. The present work aimed to obtain effective artificial peroxidase (PO)-like NZs (nanoPOs), to characterize them, and to estimate the prospects of their analytical application. NanoPOs were synthesized using a number of nanoparticles (NPs) of transition and noble metals and were screened for their catalytic activity in solution and on electrodes. The most effective nanoPOs were chosen as NZs and characterized by their catalytic activity. Kinetic parameters, size, and structure of the best nanoPOs (Cu/Ce^S) were determined. Cu/Ce^S-based sensor for H₂O₂ determination showed high sensitivity (1890 A·M⁻¹·m⁻²) and broad linear range (1.5–20,000 μM). The possibility to apply Cu/Ce^S-NZ as a selective layer in an amperometric sensor for hydrogen-peroxide analysis of commercial disinfectant samples was demonstrated.

Keywords: nanozyme; nano-peroxidase; synthesis; catalytic properties; amperometric sensors; hydrogen peroxide; disinfectant analysis



Citation: Demkiv, O.; Stasyuk, N.; Serkiz, R.; Gayda, G.; Nisnevitch, M.; Gonchar, M. Peroxidase-Like Metal-Based Nanozymes: Synthesis, Catalytic Properties, and Analytical Application. *Appl. Sci.* **2021**, *11*, 777. <https://doi.org/10.3390/app11020777>

Received: 2 December 2020

Accepted: 13 January 2021

Published: 15 January 2021

Publisher's Note: MDPI stays neutral with regard to jurisdictional claims in published maps and institutional affiliations.



Copyright: © 2021 by the authors. Licensee MDPI, Basel, Switzerland. This article is an open access article distributed under the terms and conditions of the Creative Commons Attribution (CC BY) license (<https://creativecommons.org/licenses/by/4.0/>).

1. Introduction

Peroxidase (PO; E.C. 1.11.1.7) is the oxidoreductase that catalyzes oxidation of organic substrates in the presence of hydrogen peroxide (H₂O₂) as an electron acceptor. The most popular chromogenic substrates for PO are 3,3',5,5'-tetramethylbenzidine (TMB), 2,2'-azinobis [3-ethylbenzothiazoline-6-sulfonic acid] (ABTS), and *o*-phenylenediamine (OPD). In the active site PO contains heme, an iron-porphyrin derivative [1]. The PO-mediated catalytic process occurs via a peroxidative cycle. During the PO-induced substrate oxidation in the presence of H₂O₂, the central iron is switched between the ferric(III) and intermediate ferryl(IV) states. The latter intermediate compound exhibits extremely high oxidative activity [2,3].

PO is widely used in different fields of science and industry, especially in analytics for H₂O₂ determination [1]. Many natural enzymes (oxidases) produce H₂O₂ as a byproduct of their enzymatic reactions, so that detection of the target substrates can be performed by

measuring the generation of H_2O_2 . This principle is widely used in oxidase/peroxidase-based biosensors [4,5]. To determine H_2O_2 , PO-catalyzed decomposition of H_2O_2 may be detected with optical biosensors (in the presence of chromogenic substrates) or with amperometric biosensors. The wide practical application of natural PO is still limited, however, due to the high cost of the enzyme and fast enzyme inactivation in the presence of H_2O_2 .

Artificial enzymes having PO activity, especially PO-like nanozymes (NZs) or “nanoperoxidases” (nanoPOs), are promising substitutes for natural PO, especially in biosensors [5–11]. Detailed information about NZs, including their definition, history, classification, advantages over natural enzymes, methods of obtaining them, and prospects for practical use, can be found in our recent review [12].

The catalytic properties of NZs strongly depend on the method of synthesis [12–14], chemical structure, particle size, shape, and surface morphology, which can be affected by electrical charge, coating type, doping, loading, and external fields [14–27]. The catalytic performance and efficiency of NZs are usually characterized by kinetic parameters (K_M , V_{max} , k_{cat} , k_{cat}/K_M ratio, IC_{50}) and morphological characteristics [7]. In most cases, the catalytic efficiency of NZs is lower compared to natural analogues, but some NZs can compete with natural enzymes [5–7,19].

Nanoperoxidases can be prepared in different ways, such as sol–gel, hydrothermal and solvothermal methods, electrodeposition, chemical reduction, green synthesis, pyrolysis, polymerization, polycondensation, coprecipitation, laser dewetting, and others [7,12]. For ultrafast preparation of NZs containing metal oxides of transition metals, such as $ZnCo_2O_4$, $NiCo_2O_4$, $MnCo_2O_4$, $NiMn_2O_4$, $CoCu_2O_4$, and Co_3O_4 , a new synthetic method was proposed using basic deep eutectic solvents. In this method, the designed solvents act simultaneously as a solvent, a shape-control agent and a reactant [28].

Each method of NZ synthesis has advantages and drawbacks [7,12,13]. The chemical reduction method is the most popular due to its rapidity and simplicity. The morphology and particle-size distribution of the chemically synthesized NZs may be controlled by changing molar concentration of compounds, the type of reductant, and the temperature of the reaction [29]. The faster the synthetic process is carried out, the smaller the sizes of obtained NZs, and vice versa [30]. To obtain NZs of higher purity and stronger stoichiometric control, the coprecipitation method must be chosen [31].

A number of new low-cost PO-like NZs having high catalytic activity have been described and used for the development of effective H_2O_2 -sensitive sensors [32–35]. These sensors may serve as prospective platforms in the construction of different oxidase-based biosensors for quantitative detection of different biomarkers. Biosensors with PO-like NZs can be applied in clinical diagnostics, theranostics, therapy control, and cell/tissue growth and proliferation [35–40].

In our previous studies, we demonstrated the possibility of developing reagentless amperometric biosensors using PO-like NZs. The NZs were synthesized by different methods, including electrodeposition, chemical synthesis, and green synthesis [41,42]. The most effective PO-like NZs, PtRu and hexacyanoferrate (HCF) of copper (CuHCF), were shown to be promising catalysts in amperometric (bio)sensors. When immobilized on graphite electrodes (GEs), PtRu and CuHCF were used for H_2O_2 analysis of a sample of commercial disinfectant, and for construction of oxidase-based amperometric biosensors for the determination of ethanol, methyl amine [41], and glucose [42].

Nanozymes having high mimic enzyme activities are very prospective for analytical purposes, particularly, for clinic diagnosis [6,12,13]. Most commercial diagnostic kits and biosensors use natural enzymes selective for metabolites, e.g., different oxidases and peroxidase. The latter enzyme is especially important for ELISA tests, which are very often used in clinic, food control, and sport medicine [1–5]. For this reason, synthesis of new materials capable to mimic peroxidase activity is a very important challenge for modern nanotechnology.

The aim of this work was to obtain effective NZs having PO-like activity, to characterize these nanoperoxidase NZs (nanoPOs), and to estimate the prospects of their analytical application.

The novelty of the current research is a synthesis of a broad row of hybrid metal nanoparticles (NPs) containing transition and noble metals, and a comparative study of their catalytic activity when immobilized on electrodes as well as in a solution. The latter issue is almost not related to in literature. Kinetic parameters, size, and structure of the most effective nanoPOs were determined. The Cu/Ce-based sensor for H₂O₂ determination showed the highest sensitivity (1890 A·M⁻¹·m⁻²), a broad linear range (1.5–20,000 μM), and a high current response (786 μA) upon H₂O₂ addition. The possibility to apply Cu/Ce^S-NZ as a selective layer in an amperometric sensor for hydrogen peroxide analysis in commercial disinfectant samples was demonstrated.

2. Materials and Methods

2.1. Reagents

Ascorbic acid, Ce(HCO₃)₄, AgNO₃, chloroplatinic acid (H₂PtCl₆), HAuCl₄, copper(II) sulfate (CuSO₄), zinc(II) sulfate (ZnSO₄), *o*-dianisidine, hydrogen peroxide (H₂O₂, 30%), iron(III) chloride (FeCl₃·4H₂O), palladium chloride (PdCl₃), sodium borohydride (NaBH₄), Nafion (5% solution in 90% low-chain aliphatic alcohols), and all other reagents and solvents used in this work were purchased from Sigma-Aldrich (Steinheim, Germany). All reagents were of analytical grade and were used without further purification. All solutions were prepared using ultrapure water obtained with the Milli-Q[®] IQ 7000 Water Purification system (Merck KGaA, Darmstadt, Germany).

2.2. Synthesis of NPs

NPs were synthesized by the reduction of metal ions from appropriate salts, according to the methods used in our modifications [41–44]. The conditions of NP synthesis are presented in Table 1. NPs were collected by centrifugation under 10,000 × *g* for 40 min (Hettich Micro-22R centrifuge), washed twice with water, and precipitated by centrifugation. Pellets were suspended in 0.2 mL of water and stored until use at +4 °C.

Table 1. Methods of chemical synthesis of nanoparticles.

No	NPs	Reaction Mixture and Conditions
1	Fe/Ce ^S	2 mL 50 mM FeCl ₃ + 2 mL 15 mM Ce(HCO ₃) ₄ , light stirring for 5 min at 20 °C followed by adding 0.5 mL 10 mM Na ₂ S; stirring for 1 min; incubation without stirring for 24 h at 20 °C.
2	Cu/Ce ^S	1 mL 0.01 mM Ce(HCO ₃) ₄ + 1 mL 10 mM sodium borohydride, vigorous stirring for 5 min followed by adding 2 mL 20 mM CuSO ₄ ; incubation without stirring for 1 h at 20 °C + 0.1 mL 10 mM Na ₂ S; stirring for 5 min at 20 °C.
3	Fe/Mn	2 mL 50 mM FeCl ₃ + 2 mL 50 mM MnSO ₄ , light stirring for 5 min at 20 °C followed by adding 0.5 mL 10 mM Na ₂ S; stirring for 1 min; incubation without stirring for 24 h at 20 °C.
4	Ag/Ce ^S	2 mL 50 mM AgNO ₃ + 2 mL 15 mM Ce(HCO ₃) ₄ , light stirring for 5 min followed by adding 0.1 mL 10 mM Na ₂ S; stirring for 1 min at 20 °C. incubation without stirring for 24 h at 20 °C.
5	Pt/Cu	0.2 mL 48 mM H ₂ PtCl ₆ + 0.16 mL 100 mM ascorbic acid, vigorous stirring for 5 min followed by adding 1 mL 100 mM CuSO ₄ and 0.2 mL 100 mM ascorbic acid; incubation without stirring for 24 h at 20 °C.
6	Fe/Ce	2 mL 50 mM FeCl ₃ + 2 mL 15 mM Ce(HCO ₃) ₄ , light stirring for 5 min at 20 °C followed by adding 0.5 mL 10 mM NH ₄ OH; stirring for 5 min; incubation without stirring for 24 h at 20 °C.
7	Zn/Ce	2 mL 50 mM ZnSO ₄ + 2 mL 15 mM Ce(HCO ₃) ₄ , light stirring for 5 min at 20 °C followed by adding 0.5 mL 10 mM NH ₄ OH; stirring for 5 min; incubation without stirring for 24 h at 20 °C.
8	Cu/Ce	2 mL 50 mM CuSO ₄ + 2 mL 15 mM Ce(HCO ₃) ₄ , light stirring for 5 min at 20 °C followed by adding 0.5 mL 10 mM NH ₄ OH; stirring for 5 min; incubation without stirring for 24 h at 20 °C.
9	Pd/Ce	1 mL 0.01 mM PdCl ₃ + 1 mL 100 mM NaBH ₄ , vigorous stirring for 5 min followed by adding 4 mL 0.01 mM Ce(HCO ₃) ₄ and 0.5 mL 100 mM NaBH ₄ .
10	Pd/Cu	1 mL 0.01 mM PdCl ₃ + 1 mL 10 mM NaBH ₄ , vigorous stirring for 3 min followed by adding 2 mL 0.01 mM Ce(HCO ₃) ₄ and 0.5 mL 100 mM NaBH ₄ ; stirring for 1 min; incubation without stirring for 24 h at 20 °C.

Table 1. Cont.

No	NPs	Reaction Mixture and Conditions
11	Ag/Ce	2 mL 50 mM AgNO ₃ + 2 mL 15 mM Ce(HCO ₃) ₄ , vigorous stirring for 5 min at 20 °C followed by adding 0.1 mL 100 mM NaBH ₄ ; stirring for 5 min; incubation without stirring for 24 h at 20 °C.
12	Au/Cu	2 mL 50 mM CuSO ₄ + 2 mL 15 mM Ce(HCO ₃) ₄ , vigorous stirring for 5 min at 20 °C followed by adding 0.1 mL 100 mM NaBH ₄ ; stirring for 5 min; incubation without stirring for 24 h at 20 °C.
13	Au	0.145 mL 58.5 mM HAuCl ₄ + 10 mL 10 mM CTAB, vigorous stirring; + 0.18 mL 100 mM NaBH ₄ ; stirring for 2 h at 20 °C.
14	Ag/Cu	2 mL 50 mM CuSO ₄ + 2 mL AgNO ₃ , vigorous stirring for 5 min at 20 °C followed by adding 0.1 mL 100 mM NaBH ₄ ; incubation without stirring for 24 h at 20 °C.
15	Pt/Ag	0.2 mL 48 mM H ₂ PtCl ₆ + 2 mL AgNO ₃ , vigorous stirring for 5 min at 20 °C followed by adding 0.1 mL 100 mM NaBH ₄ ; stirring for 5 min; incubation without stirring for 24 h at 20 °C.
16	Ag/Zn	2 mL 50 mM AgNO ₃ + 2 mL 50 mM ZnSO ₄ , vigorous stirring for 5 min at 20 °C followed by adding 0.1 mL 100 mM NaBH ₄ ; stirring for 5 min; incubation without stirring for 24 h at 20 °C.

^S—NPs obtained by a sulfide method.

2.3. Morphological Analysis of NPs Using Scanning Electron Microscopy (SEM)

Morphological analyses of the samples were performed using a SEM microanalyzer (REMMA-102-02, Sumy, Ukraine). The samples in different dilutions (2 µL) were dropped onto the surface of a silicon wafer and were dried at room temperature. The distance from the last lens of the microscope to the sample (WD) ranged from 17.1 mM to 21.7 mM. The accelerator voltage was in the range of 20 to 40 eV.

2.4. Determination of Peroxidase-Like Activity of NPs in Solution

PO-like activity of the NPs was measured by the colorimetric method, with *o*-dianisidine as a chromogenic substrate in the presence of H₂O₂. The generated color was determined at 525 nm using a Shimadzu UV1650 PC spectrophotometer (Kyoto, Japan). One unit (U) of PO-like activity was defined as the amount of NZ releasing 1 µMol H₂O₂ per 1 min at 30 °C under standard assay conditions.

The procedure of the PO-like activity assay: 10 µL of the aqueous suspension of NPs (1 mg/mL) was incubated in a glass tube with 1 mL of 0.17 mM *o*-dianisidine in 50 mM NaOAc buffer, pH 4.5 (as a control); and with the same substrate in the presence of 8.8 mM H₂O₂ (as a substrate for PO). Addition of NPs to the substrate stimulated the development of an orange color over time, indicating an enzymatic reaction. The enzyme-mimetic activity could be assessed qualitatively with the naked eye and was measured quantitatively with a spectrophotometer. After incubation for an exact time (1–10 min) at 30 °C, and upon appearance of the orange color, the reaction was stopped by the addition of 0.26 mL 12 M HCl. The millimolar extinction coefficient of the resulting pink dye in the acidic solution was 13.38 mM⁻¹·cm⁻¹.

2.5. Sensor Evaluation

2.5.1. Apparatus, Measurements, and Statistical Analysis

The amperometric sensors were evaluated using constant-potential amperometry in a three-electrode configuration with an Ag/AgCl/KCl (3 M) reference electrode, a Pt-wire counter electrode, and a graphite working electrode. Graphite rods (type RW001, 3.05 mm diameter) from Ringsdorff Werke (Bonn, Germany) were sealed in glass tubes using epoxy glue to form disk electrodes. Before sensor preparation, the graphite electrode (GE) was polished with emery paper and a polishing cloth using decreasing particle sizes of alumina paste (Leco, Germany). The polished electrodes were rinsed with water in an ultrasonic bath.

Amperometric measurements were carried out using a CHI 1200A potentiostat (IJ Cambria Scientific, Burry Port, UK) connected to a personal computer and performed in a batch mode under continuous stirring in an electrochemical cell with a 20 mL volume at 25 °C.

All the experiments were carried out in triplicate trials. Analytical characteristics of the electrodes were statistically processed using OriginPro 8.5 software. The error bars represent the standard error derived from three independent measurements. Calculation of the apparent Michaelis–Menten constants (K_M^{app}) was performed automatically by this program according to the Lineweaver–Burk equation.

2.5.2. Immobilization of Metallic NPs onto Electrodes, Testing Their Electro- and PO-Like Activity

For construction of the NZ-based electrode, 5 μ L of NP suspension (1 mg/mL) was dropped onto the surfaces of GEs. After drying for 10 min at room temperature, the layer of NPs on the electrodes was covered with 5 μ L Nafion membrane. The electrodes were washed with corresponding buffer solutions before and after each measurement.

The electrochemical properties of the synthesized NPs were studied by cyclic voltammetry (CV) on the GEs in the range from -1000 to $+1000$ mV with the scan rate of 50 mV min^{-1} ; the profiles of amperometric signals in increasing concentrations of H_2O_2 were compared. The most electroactive NPs, which had the highest PO-like properties, were chosen for further investigation.

3. Results and Discussion

3.1. Obtaining and Characterizing the Best Peroxidase-Like Nanozymes

First, different NPs were synthesized and screened for their reaction to H_2O_2 in solution. PO-like activities were measured with *o*-dianisidine as the chromogenic substrate. The experiments demonstrated that the synthesized NPs, especially Au/Cu, Ag/Ce^S, Fe/Ce^S, and Zn/Ce, possessed significant PO-like activities in solution (Table 2). These results are in agreement with the data of other researchers [9,10].

Table 2. Peroxidase (PO)-like activities of the synthesized nanozymes NZs in solution.

No.	Nanozyme	Synthesis Method	Specific Activity, Units /mg
1	Fe/Ce ^S	Na ₂ S	1.86 ± 0.16
2	Cu/Ce ^S	NaBH ₄ /Na ₂ S	1.27 ± 0.11
3	Fe/Mn	Na ₂ S	0.12 ± 0.01
4	Ag/Ce ^S	Na ₂ S	0.05 ± 0.004
5	Pt/Cu	Ascorbic acid	1.84 ± 0.14
6	Fe/Ce	NH ₄ OH	3.06 ± 0.26
7	Zn/Ce	NH ₄ OH	2.28 ± 0.21
8	Cu/Ce	NH ₄ OH	0.90 ± 0.007
9	Pd/Ce	NaBH ₄	0.72 ± 0.06
10	Pd/Cu	NaBH ₄	0.4 ± 0.03
11	Ag/Ce	NaBH ₄	2.50 ± 0.22
12	Au/Cu	NaBH ₄	4.22 ± 0.34
13	Au	NaBH ₄	2.62 ± 0.19
14	Ag/Cu	NaBH ₄	0.24 ± 0.02
15	Pt/Ag	NaBH ₄	1.40 ± 0.11
16	Ag/Zn	NaBH ₄	0.79 ± 0.06

^S—NPs obtained by a sulfide method.

The most catalytically active NZs were characterized by SEM coupled with X-ray microanalysis (SEM-XRM). SEM provided information on the size, distribution, and shape of the tested sample. Figure S1 presents the overall morphology of the formed hybrid particles. The XRM images of the synthesized NZs showed the characteristic peaks for metals of the composites.

The obtained Pd/Ce NPs have the shape of a sphere with a diameter of approximately 200 nm. The size of synthesized Pt/Cu NPs is near 500 nm. XRM data for Pt/Cu NPs proved the presence of Pt⁰ and Cu⁰ forms, with characteristic peaks $K\alpha$ at 2.4 keV and 1.4 keV, respectively (Figure S1). The size of synthesized Pd/Cu NPs is in the range of

500 nm–1 μM . The sole peak at 1.8 keV demonstrates the full covering of CuNPs with the PdNPs.

SEM imaging and XRM data proved the formation of needlelike hybrid Fe/Ce and Au/Cu micro particles with the size ranging from 10 to 20 μM (Figure S1). The XRM image of Au/Cu NPs shows the $K\alpha$ peaks of Cu^0 and Au^0 , confirming the presence of both CuNPs and AuNPs. It was shown that the Fe/Ce and Au/Cu NPs tested look like irregular shaped clusters of microfibrillar structures. The best of catalytically active NZs, namely, Cu/CeS, Au/Cu, Ag/Ce, Fe/Ce, Ag/Zn, Pd/Ce, and Pt/Cu NPs were chosen for further investigation.

3.2. Development and Characterization of the NZs-Modified Electrodes

Our next task was to select the most PO-active NPs immobilized on the electrode surface. It is known that modification of an electrode with some metallic NPs can improve the efficiency of an electron transfer, due to an increase in the electrochemically accessible electrode surface area. Numerous NZs/GEs were screened for their ability to decompose hydrogen peroxide. The electrocatalytic activities of the synthesized NZs, while immobilized on the surface of GEs, were tested by CV and chronoamperometry, as described in Section 2.5.2 (Figure 1 and Figure S2).

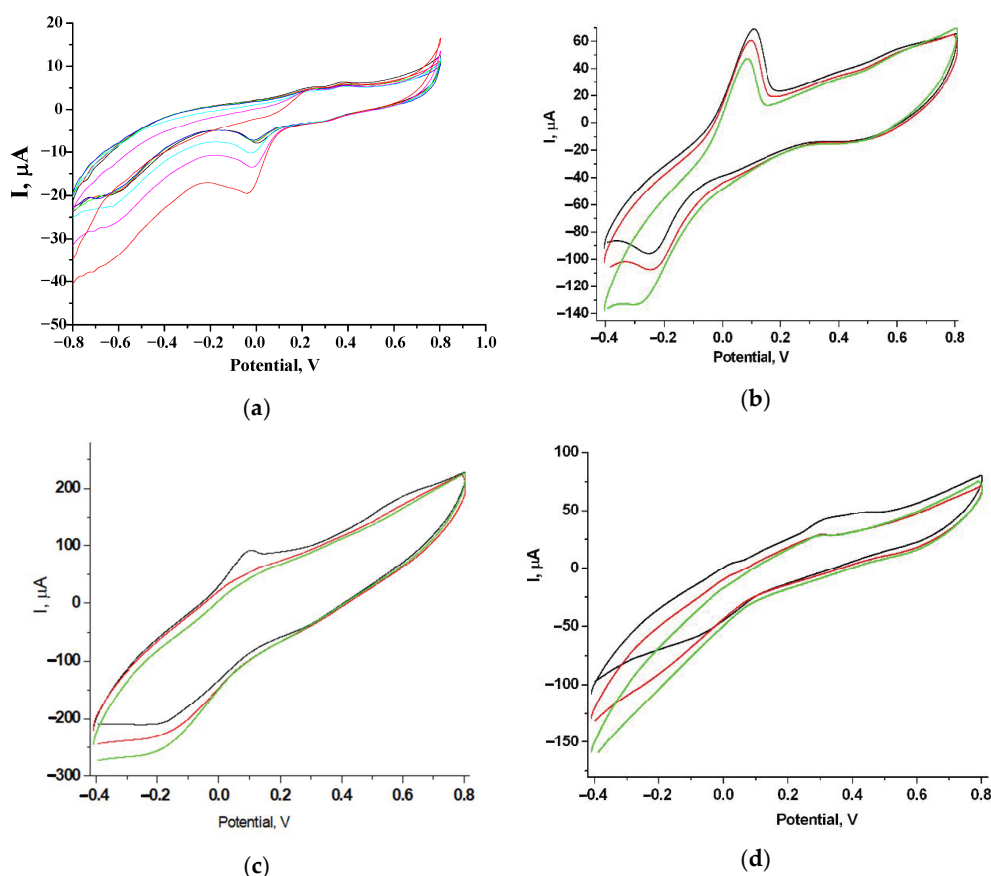


Figure 1. Cyclic voltammograms (CV) of the graphite electrodes modified with Cu/Ce^S (a), Fe/Ce (b), Au/Cu (c), and Ag/Ce (d). CV profiles as outputs on addition of H₂O₂ in concentration: (a)—0 mM (blue), 0.2 mM (cyan), 0.5 mM (pink), 1 mM (red); (b–d)—0 mM (black), 1 mM (red), 3 mM (green). Conditions: scan rate 50 mV·s⁻¹; Ag/AgCl (reference electrode) in 50 mM NaOAc buffer, pH 4.5. The surfaces of the graphite electrode (GE) were modified with 1 μg (a) or 5 μg NZs (b–d) and covered with Nafion.

In our research, the amperometric responses of different NZs/GEs to added portions of H₂O₂ were compared under mild conditions at the working potential of -50 mV. This rather low potential was chosen from the CV profiles (Figure 1), since the main drawback

of many H_2O_2 -sensitive NZ-based electrochemical sensors is their nonselectivity under high positive (or negative) working potentials. H_2O_2 is able to direct the auto-oxidation on electroactive surfaces at a working potential above +0.4 V, or auto-reduction at -0.4 V or less vs. Ag/AgCl. Moreover, the real samples containing organic compounds may be easily co-oxidized/co-reduced at extreme potentials, which may result in overestimation of the target analytes in the presence of oxygen. To avoid these problems during sensor analysis, it was important to screen new NZs while working at operating potentials close to zero (0) V vs. Ag/AgCl [12,43–45]. This requirement is especially relevant for the construction of biosensors and their exploitation for analysis of real samples (food products, biological liquids, etc.). Our previous experiments with natural PO as a biorecognition element of amperometric biosensors were also carried out at -50 mV [41–44].

Using the chronoamperograms, calibration curves were plotted for H_2O_2 determination by the developed electrodes (Figure S2). The analytical characteristics of the modified GEs, as deduced from the graphs in comparison with natural PO [42–44], are summarized in Table 3. The linear ranges, limits of detection (LOD), and sensitivities of the electrodes modified with nanoPOs were calculated. The limit of blank values (LOB) for NZ was calculated as $0.3 \times \text{LOD}$. The sensitivity of each NZ-modified electrode was measured for an electrode area of 7.30 mm^2 .

Table 3. Analytical characteristics of the most effective NZs as PO-mimetic placed on electrode.

Sensitive Film	No. in Table 2	Sensitivity, $\text{A M}^{-1} \text{m}^{-2}$	LOD, μM	Linear Range, μM	K_M^{app} , mM	I_{max} , μA
PO		352		400	4.9 ± 1.1	5.0 ± 0.2
Cu/Ce ^S	2	1890	0.42 ± 0.006	1.5–20,000	43.3 ± 14.5	786.4 ± 167.7
Fe/Ce	6	1372	2.90 ± 0.010	50–1000	14.4 ± 1.3	104.5 ± 3.3
Au/Cu	12	793	4.88 ± 0.010	50–15,000	28.0 ± 3.2	213.3 ± 13.1
Ag/Ce	11	782	11 ± 0.009	50–4000	16.4 ± 2.5	152.54 ± 8.8
Pd/Cu	10	581	39 ± 1.20	117–14,300	34.7 ± 2.02	166.2 ± 6.4
Pd/Ce	9	496	4.55 ± 0.006	17–4100	13.4 ± 3.2	68.0 ± 3.2
Ag/Zn	16	375	41 ± 1.50	17–25,000	18.1 ± 0.4	96.79 ± 8.56
Pt/Cu	5	163	5.54 ± 0.002	17–25,000	26.8 ± 5.0	55.2 ± 5.4

^S—NPs obtained by a sulfide method.

Figure 2 summarizes the data concerning the PO-like properties of the selected NZs, namely, Cu/Ce^S, Au/Cu, Ag/Ce, Fe/Ce, Ag/Zn, Pd/Ce, and Pt/Cu. The results in Table 3 demonstrate that Cu/Ce^S/GE exhibited the highest sensitivity ($1890 \text{ A} \cdot \text{M}^{-1} \cdot \text{m}^{-2}$) and current response ($786 \mu\text{A}$), the lowest LOD ($0.42 \mu\text{M}$), and a broad linear range ($1.5\text{--}20,000 \mu\text{M}$) upon H_2O_2 addition. This structure was therefore studied in more detail as the most effective artificial PO immobilized on the electrode.

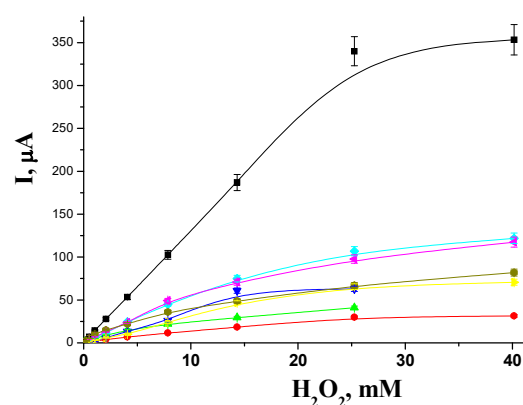


Figure 2. Dependence of the current response on increasing concentrations of H_2O_2 for GEs modified with $5 \mu\text{g}$ of different nanozymes: Cu/Ce^S (black line), Au/Cu (cyan), Ag/Ce (violet), Fe/Ce (khaki), Ag/Zn (yellow), Pd/Ce (green), Pt/Cu (red).

3.3. Characterization of the Most Effective Cu/Ce^S-Modified Electrode

The Cu/Ce^S-NZ with the highest PO-like activity was studied in detail. The Cu/Ce^S/GE demonstrated the highest PO-like activity, compared with other NZs and with natural PO (Figure S2, Tables 3 and 4). The highest current response (I_{max}) on the tested analyte at substrate saturation of the Cu/Ce^S/GE was 157-fold higher, and its sensitivity was 5.4-fold higher, than that of the PO/GE (Table 3). It is worth mentioning that Cu/Ce^S has PO-like ability but lacks oxidase (laccase)-like properties. This conclusion was reached from the results of colorimetric tests using *o*-dianisidine in the presence of H₂O₂ as a substrate for PO, and with *o*-dianisidine only as a substrate for oxidase (see Section 2.4). The Cu/Ce^S specificity to H₂O₂ is the important valuable characteristic for applying it as a selective PO-mimetic element in sensors and oxidase-based biosensors. Figure 3 shows the effect of quantity on the NZ immobilized on the GE surface, based on the amperometric signal as a response to H₂O₂ addition. Table 4 presents comparative analytical characteristics of the recently developed metallic NZ-based sensors for H₂O₂ analysis, including the results described here.

Table 4. The main operational characteristics of the recently described H₂O₂-sensitive metallic NZ-based sensors working at low potentials.

Electrode	PO Mimetic	Potential, mV	Sensitivity, A M ⁻¹ m ⁻²	Linear Range, μM	Ref.
¹ GCE	Cu ₂ O/PANI/rGhO	−200	394	0.8–12,780	[45]
GCE	Fe ₃ O ₄ /3D GNCs	−200	2742	0.8–330	[46]
GCE	Ni-Fe PBA- ⁴ HNCs	−50	361	0.1–20,000	[47]
GCE	PB/BG	−50	2852	4–830	[48]
	AuNPs-PB/BG	−50	11,243	9.2–8100	
² DBD	PB		2100		
DBD	Ni-FePBA	−50	1500	0.5–1000	[11]
GE	PB/NZ		4500		
GCE	MnPBA		1472	3–8610	[49]
GCE	rGhO/Pt-Ag	−50	6996	5–1500	[50]
GCE	Ni-PB	−50	3500	0.1–1000	[51]
Graphite paste	Ni-FePBA	−50	1130	2–1000	[52]
	Cu-FePBA	−50	2030	0.5–1000	
³ GE	PtRu	−50	194	17–25,000	[41]
GE	gCuHCF		1620	16–4100	
	gFeHCF	−50	1090	116–14,300	[42]
	PO		352	15–20,000	
GCE	Ni-FePBA	0	18,000	up to 100	[53]
GCE	PNAANI-PB	0	5073	1–1000	[54]
GCE	PB	50	6000	0.1–100	[55]
GCE	Fe/rGhO-Pt	100	3400	7.5–4270	[56]
GCE	PB	180	10,000/20,000	1–5000	[57]
GE	Cu/Ce ^S		1890	1.5–20,000	
	Au/Cu	−50	793	17–15,000	
	Fe/Ce	-	1372	up to 1000	This paper

¹ GCE—glassy carbon electrode; ² DBD—diamond boron-doped; ³ GE—graphite electrode; ⁴ HNCs—hollow nanocubes.

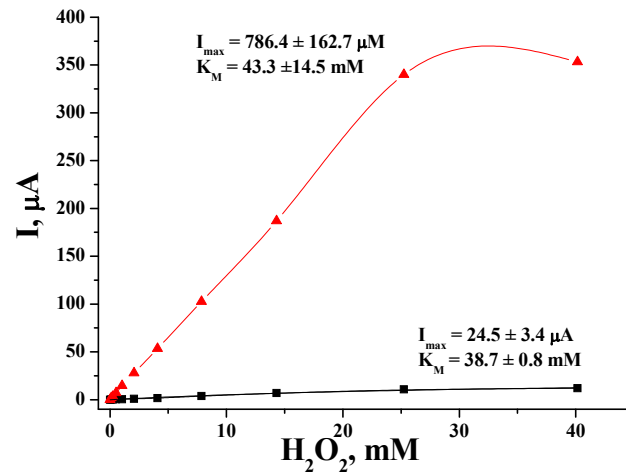


Figure 3. Dependence of the current response on increasing concentrations of H₂O₂ for GEs modified with different quantities of Cu/Ce^S: 1 μg (black line) and 5 μg (red line).

3.4. Application of Cu/Ce^S as a PO-Mimetic in Amperometric Sensors

To demonstrate the applicability of Cu/Ce^S as a chemosensor for H₂O₂ detection, analysis of H₂O₂ concentration was carried out in samples of commercial products (Figure 4). The disinfectant samples tested were Famidez–Sanosil, Spray Antiseptic for arms and a pharmaceutical solution of 3% H₂O₂. The standard addition test, SAT, approach was used to avoid undesirable effects on analytical results from additives in the tested solutions.

Graphical SAT is a type of quantitative analysis often used in analytical chemistry when a standard is added directly to the aliquots of the analyzed sample. SAT is used in situations where sample components may contribute to the analytical signal, thus making it impossible to use a routine calibration method. Estimation of H₂O₂ in the initial sample was performed using the equation $C = AN/B$, where A and B are parameters of a linear regression and N is the dilution factor.

The results of hydrogen peroxide determination in commercial samples in comparison to data of manufacturers are presented in Table 5. The average H₂O₂ concentrations determined from the data in Figure 4 correlated well with the manufacturer's data (Table 5), with an error of less than 10%.

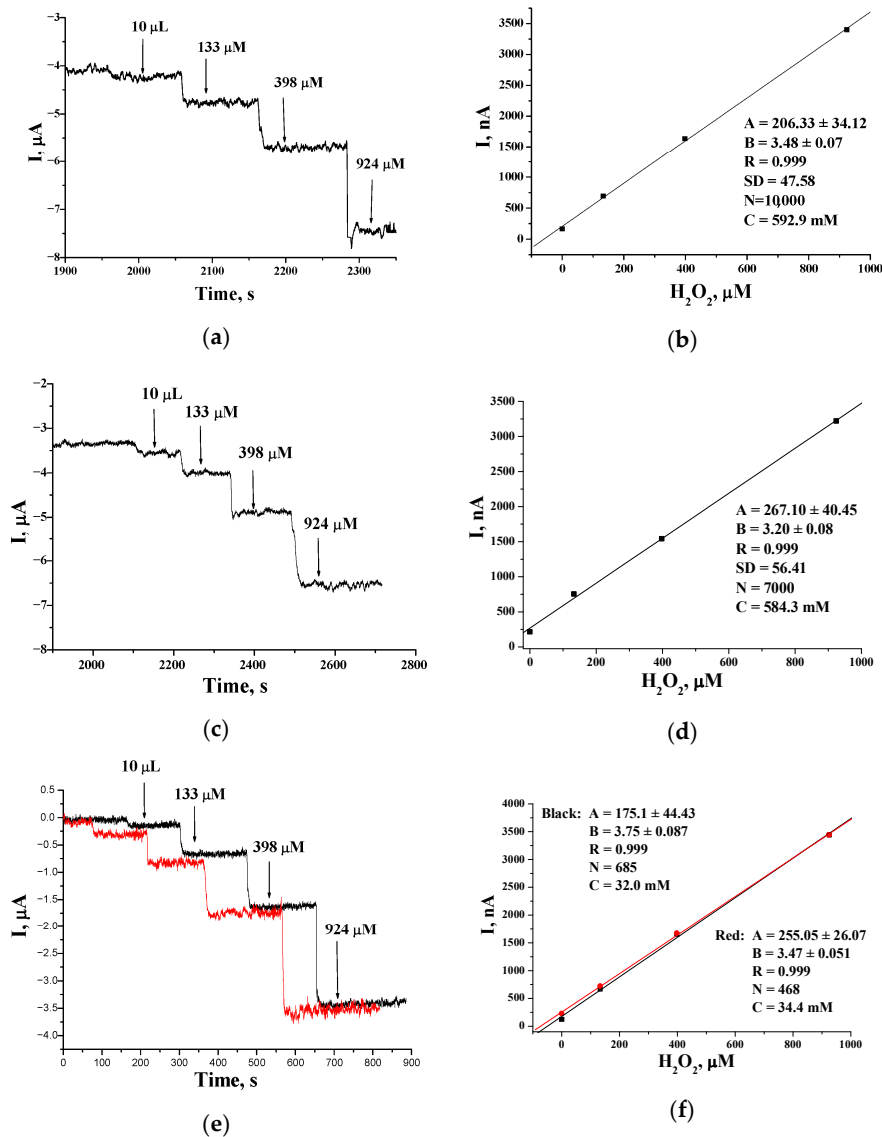


Figure 4. Analysis of the real samples of disinfectants using Cu/Ce^S-based chemosensor with the SAT method: chronoamperograms (a,c,e) and correspondent linear graphs (b,d,f). Disinfectants: Famidez-Sanosil (a–d); antiseptic spray (e,f). Analytical conditions: working potential—50 mV vs. Ag/AgCl (reference electrode), 50 mM NaOAc buffer, pH 4.5 at 23 °C.

Table 5. Results of H₂O₂ estimation in H₂O₂-containing commercial disinfectants.

Commercial Sample	Concentration of H ₂ O ₂		CV, %	Producer
	Estimated mM	Declared, %		
Antiseptic spray for arms	33.2	0.11	10.0	Pharmaceutical factory “Viola”, Zaporizhzhia, Ukraine
Universal antiseptic solution	880	2.95	1.7	
Famidez–Sanosil	588.6	1.98	1.0	Ltd Dezomark, Novoyavorivsk, Ukraine

4. Conclusions

In the current research, a number of NPs based on transition and noble metals were synthesized by chemical methods and were screened for their ability to decompose hydro-

gen peroxide in solutions. Structure, size, morphology, composition, catalytic properties, and electrochemical activities of the chosen PO-like NZs were characterized on the electrode. A more detailed study was performed for Cu/Ce^S-NZ, which was found to be the most effective mimetic of PO. It was demonstrated that the synthesized Cu/Ce^S-NZ may be successfully used as an artificial PO for sensor analysis of hydrogen peroxide in commercial disinfectant samples.

Supplementary Materials: The following are available online at <https://www.mdpi.com/2076-3417/11/2/777/s1>, Figure S1: Characteristics of the several metallic PO-like nanozymes: SEM images at different magnifications (top) and their X-ray spectral characteristics (bottom); Figure S2: Amperometric characteristics of the several NZ-modified electrodes: chronoamperograms (left), dependence of the current response on increasing concentrations of H₂O₂ (middle) and calibration graphs (right). Conditions: working potential −50 mV vs. Ag/AgCl (reference electrode), 50 mM NaOAc buffer, pH 4.5 at 23 °C.

Author Contributions: Conceptualization: G.G. and M.N.; methodology: N.S., O.D. and G.G.; investigation: O.D., R.S. and N.S.; resources: M.G.; data curation: G.G.; writing—original draft preparation: G.G., N.S. and O.D.; writing—review and editing: G.G. and M.N.; supervision: M.G.; project administration: G.G.; funding acquisition: M.G. and M.N. All authors have read and agreed to the published version of the manuscript.

Funding: This work was partially funded by NAS of Ukraine (The program “Smart sensor devices of a new generation based on modern materials and technologies”), by the Ministry of Education and Science of Ukraine (Ukrainian–Lithuanian R&D, project 0120U103398), by National Research Foundation of Ukraine (project 48/02.2020 “Development of new nanozymes as catalytic elements for enzymatic kits and chemo/biosensors”) and by the Research Authority of the Ariel University, Israel.

Institutional Review Board Statement: “Not applicable” for studies not involving humans.

Informed Consent Statement: “Not applicable” for studies not involving humans.

Data Availability Statement: “Not applicable” for studies not involving humans.

Acknowledgments: We acknowledge Mariya F. Ivash (Institute of Cell Biology, Lviv, Ukraine) for technical support and experimental assistance.

Conflicts of Interest: The authors declare no conflict of interest.

Abbreviations

2,4-DCP	2,4-Dichlorophenol
ABTS	2,2'-Azinobis-(3-ethylbenzthiazoline-6-sulphonate)
CV	Cyclic voltammetry
DBD	Diamond boron-doped
gCuHCF	Hexacyanoferrate of coppers obtained via enzyme
GCE	Glassy carbon electrode
GE	Graphite electrode
HNCs	Hollow nanocubes
I_{max}	Maximal current response on tested analyte at substrate saturation
K_M^{app}	Apparent Michaelis–Menten constant
LOD	Limit of detection
LR	Linear range
MOFs	Metal–Organic Frameworks
NPs	Nanoparticles
NZ	Nanozyme
Me/Ce ^S	Nanozyme obtained in the presence of Na ₂ S in reaction mixture; where Me–Fe, Cu or Ag.
OPD	<i>o</i> -Phenylenediamine
PO	Natural horseradish peroxidase
SAT	Standard addition test
SEM-XRM	Scanning electron microscopy coupled with X-ray microanalysis
TMB	3,5,3',5'-Tetramethylbenzidine

References

1. Dunford, H.B. *Heme Peroxidases (University of Alberta)*; Wiley-VCH, John Wiley and Sons: New York, NY, USA, 1999; 507p, ISBN 0-471-24244-6.
2. Veitch, N.C.; Smith, A.T. Horseradish peroxidase. *Comput. Chem.* **2000**, *51*, 107–162. [[CrossRef](#)]
3. Plieth, C. Peroxide-Induced Liberation of Iron from Heme Switches Catalysis during Luminol Reaction and Causes Loss of Light and Heterodyning of Luminescence Kinetics. *ACS Omega* **2019**, *4*, 3268–3279. [[CrossRef](#)] [[PubMed](#)]
4. Tatsuma, T.; Watanabe, T. Peroxidase model electrodes: Heme peptide modified electrodes as reagentless sensors for hydrogen peroxide. *Anal. Chem.* **1991**, *63*, 1580–1585. [[CrossRef](#)] [[PubMed](#)]
5. Neumann, B.; Wollenberger, U. Electrochemical Biosensors Employing Natural and Artificial Heme Peroxidases on Semiconductors. *Sensors* **2020**, *20*, 3692. [[CrossRef](#)]
6. Attar, F.; Shahpar, M.G.; Rasti, B.; Sharifi, M.; Saboury, A.A.; Rezayat, S.M.; Falahati, M. Nanozymes with intrinsic peroxidase-like activities. *J. Mol. Liq.* **2019**, *278*, 130–144. [[CrossRef](#)]
7. Wu, J.; Wang, X.; Wang, Q.; Lou, Z.; Li, S.; Zhu, Y.; Qin, L.; Wei, H. Nanomaterials with enzyme-like characteristics (nanozymes): Next-generation artificial enzymes (II). *Chem. Soc. Rev.* **2019**, *48*, 1004–1076. [[CrossRef](#)]
8. Gallay, P.; Eguílaz, M.; Rivas, G.A. Designing electrochemical interfaces based on nanohybrids of avidin functionalized-carbon nanotubes and ruthenium nanoparticles as peroxidase-like nanozyme with supramolecular recognition properties for site-specific anchoring of biotinylated residues. *Biosens. Bioelectron.* **2020**, *148*, 111764. [[CrossRef](#)]
9. Sun, L.; Ding, Y.; Jiang, Y.; Liu, Q. Montmorillonite-loaded ceria nanocomposites with superior peroxidase-like activity for rapid colorimetric detection of H₂O₂. *Sens. Actuators B Chem.* **2017**, *239*, 848–856. [[CrossRef](#)]
10. Cui, F.; Deng, Q.; Sun, L. Prussian blue modified metal–organic framework MIL-101(Fe) with intrinsic peroxidase-like catalytic activity as a colorimetric biosensing platform. *RSC Adv.* **2015**, *5*, 98215–98221. [[CrossRef](#)]
11. Komkova, M.A.; Pasquarelli, A.; Andreev, E.A.; Galushin, A.A.; Karyakin, A.A. Prussian Blue modified boron-doped diamond interfaces for advanced H₂O₂ electrochemical sensors. *Electrochim. Acta* **2020**, *339*, 135924. [[CrossRef](#)]
12. Stasyuk, N.; Smutok, O.; Demkiv, O.M.; Prokopiv, T.; Gayda, G.Z.; Nisnevitch, M.; Gonchar, M.V. Synthesis, Catalytic Properties and Application in Biosensors of Nanozymes and Electronanocatalysts: A Review. *Sensors* **2020**, *20*, 4509. [[CrossRef](#)] [[PubMed](#)]
13. Qin, L.; Hu, Y.; Wei, H. Nanozymes: Preparation and Characterization. In *Nanotechnology for Electronics, Photonics, and Renewable Energy*; Springer Science and Business Media LLC: Berlin/Heidelberg, Germany, 2020; pp. 79–101.
14. Yue, Y.; Wei, H.; Guo, J.; Yang, Y. Ceria-based peroxidase-mimicking nanozyme with enhanced activity: A coordination chemistry strategy. *Colloids Surf. A Physicochem. Eng. Asp.* **2021**, *610*, 125715. [[CrossRef](#)]
15. Wang, Z.; Zhang, R.; Yan, X.; Fan, K. Structure and activity of nanozymes: Inspirations for de novo design of nanozymes. *Mater. Today* **2020**, *41*, 81–119. [[CrossRef](#)]
16. Wang, Y.; Mao, J.; Meng, X.; Yu, L.; Deng, D.; Bao, X. Catalysis with Two-Dimensional Materials Confining Single Atoms: Concept, Design, and Applications. *Chem. Rev.* **2019**, *119*, 1806–1854. [[CrossRef](#)]
17. Shen, J.; Shafiq, M.; Ma, M.; Chen, H. Synthesis and Surface Engineering of Inorganic Nanomaterials Based on Microfluidic Technology. *Nanomaterials* **2020**, *10*, 1177. [[CrossRef](#)]
18. Huang, Y.; Ren, J.; Qu, X. Nanozymes: Classification, Catalytic Mechanisms, Activity Regulation, and Applications. *Chem. Rev.* **2019**, *119*, 4357–4412. [[CrossRef](#)]
19. Chen, J.; Qiu, H.; Zhao, S. Fabrication of chemiluminescence resonance energy transfer platform based on nanomaterial and its application in optical sensing, biological imaging and photodynamic therapy. *TrAC Trends Anal. Chem.* **2020**, *122*, 115747. [[CrossRef](#)]
20. Rauf, S.; Ali, N.; Tayyab, Z.; Shah, M.A.K.Y.; Yang, C.P.; Hu, J.; Kong, W.; Huang, Q.; Hayat, A.; Muhammad, N. Ionic liquid coated zerovalent manganese nanoparticles with stabilized and enhanced peroxidase-like catalytic activity for colorimetric detection of hydrogen peroxide. *Mater. Res. Express* **2020**, *7*, 035018. [[CrossRef](#)]
21. Zhang, K.; Zuo, W.; Wang, Z.; Liu, J.; Li, T.; Wang, B.; Yang, Z. A simple route to CoFe₂O₄ nanoparticles with shape and size control and their tunable peroxidase-like activity. *RSC Adv.* **2015**, *5*, 10632–10640. [[CrossRef](#)]
22. Liu, B.; Liu, J. Surface modification of nanozymes. *Nano Res.* **2017**, *10*, 1125–1148. [[CrossRef](#)]
23. Zhao, M.; Huang, J.; Zhou, Y.; Pan, X.; Chen, Z.; Ye, Z.; Pan, X. Controlled synthesis of spinel ZnFe₂O₄ decorated ZnO heterostructures as peroxidase mimetics for enhanced colorimetric biosensing. *Chem. Commun.* **2013**, *49*, 7656–7658. [[CrossRef](#)] [[PubMed](#)]
24. Liu, C.; Yan, Y.; Zhang, X.; Mao, Y.; Ren, X.; Hu, C.; He, W.; Yin, J.-J. Regulating the pro- and anti-oxidant capabilities of bimetallic nanozymes for the detection of Fe²⁺ and protection of Monascus pigments. *Nanoscale* **2020**, *12*, 3068–3075. [[CrossRef](#)] [[PubMed](#)]
25. Liu, M.; Kong, L.; Wang, X.; He, J.; Bu, X.-H. Engineering Bimetal Synergistic Electrocatalysts Based on Metal–Organic Frameworks for Efficient Oxygen Evolution. *Small* **2019**, *15*, e1903410. [[CrossRef](#)] [[PubMed](#)]
26. Cao-Milán, R.; He, L.D.; Shorkey, S.; Tonga, G.Y.; Wang, L.-S.; Zhang, X.; Uddin, I.; Das, R.; Sulak, M.; Rotello, V.M. Modulating the catalytic activity of enzyme-like nanoparticles through their surface functionalization. *Mol. Syst. Des. Eng.* **2017**, *2*, 624–628. [[CrossRef](#)]
27. Wang, X.; Hu, Y.; Wei, H. Nanozymes in bionanotechnology: From sensing to therapeutics and beyond. *Inorg. Chem. Front* **2016**, *3*, 41–60. [[CrossRef](#)]

28. Chen, J.; Wei, X.; Tang, H.; Munyemana, J.C.; Guan, M.; Zhang, S.; Qiu, H. Deep eutectic solvents-assisted synthesis of ZnCo₂O₄ nanosheets as peroxidase-like nanozyme and its application in colorimetric logic gate. *Talanta* **2021**, *222*, 121680. [[CrossRef](#)]
29. Rane, A.V.; Kanny, K.; Abitha, V.K.; Sabu, T. Chapter 5. Methods for Synthesis of Nanoparticles and Fabrication of Nanocomposites. In *Synthesis of Inorganic Nanomaterials Advances and Key Technologies Micro and Nano Technologies*, 1st ed.; Bhagyaraj, S.M., Oluwafemi, O.S., Kalarikkal, N., Sabu, T., Eds.; Woodhead Publishing Company: Sawston, UK, 2018; pp. 121–139. ISBN 9780081019757.
30. Suriati, G.; Mariatti, M.; Azizan, A. Synthesis of silver nanoparticles by chemical reduction method: Effect of reducing agent and surfactant concentration. *Int. J. Automot. Mech. Eng.* **2014**, *10*, 1920–1927. [[CrossRef](#)]
31. Chen, H.-I.; Chang, H.-Y. Synthesis of nanocrystalline cerium oxide particles by the precipitation method. *Ceram. Int.* **2005**, *31*, 795–802. [[CrossRef](#)]
32. Vokhmyanina, D.V.; Andreeva, K.D.; Komkova, M.A.; Karyakina, E.E.; Karyakin, A.A. ‘Artificial peroxidase’ nanozyme–enzyme based lactate biosensor. *Talanta* **2020**, *208*, 120393. [[CrossRef](#)]
33. Neampet, S.; Ruecha, N.; Qin, J.; Wonsawat, W.; Chailapakul, O.; Rodthongkum, N. A nanocomposite prepared from platinum particles, polyaniline and a Ti3C2 MXene for amperometric sensing of hydrogen peroxide and lactate. *Microchim. Acta* **2019**, *186*, 752. [[CrossRef](#)]
34. Matos-Peralta, Y.; Antuch, M. Review—Prussian Blue and Its Analogs as Appealing Materials for Electrochemical Sensing and Biosensing. *J. Electrochem. Soc.* **2019**, *167*, 037510. [[CrossRef](#)]
35. Meng, X.; Gao, L.; Fan, K.; Yan, X. *Nanozyme-Based Tumor Theranostics*; Springer Science and Business Media LLC: Berlin/Heidelberg, Germany, 2020; pp. 425–457.
36. Chen, W.; Gao, G.; Jin, Y.; Deng, C. A facile biosensor for Aβ₄₀ based on fluorescence quenching of prussian blue nanoparticles. *Talanta* **2020**, *216*, 120930. [[CrossRef](#)] [[PubMed](#)]
37. He, L.; Li, Z.; Guo, C.; Hu, B.; Wang, M.; Du, M.; Du, M. Bifunctional bioplatfrom based on NiCo Prussian blue analogue: Label-free impedimetric aptasensor for the early detection of carcino-embryonic antigen and living cancer cells. *Sens. Actuators B Chem.* **2019**, *298*, 126852. [[CrossRef](#)]
38. Tabrizi, M.A.; Shamsipur, M.; Saber, R.; Sarkar, S.; Zolfaghari, N. An ultrasensitive sandwich-type electrochemical immunosensor for the determination of SKBR-3 breast cancer cell using rGO-TPA/FeHCFnano labeled Anti-HCT as a signal tag. *Sens. Actuators B Chem.* **2017**, *243*, 823–830. [[CrossRef](#)]
39. Jiang, D.; Ni, D.; Rosenkrans, Z.T.; Huang, P.; Yan, X.; Cai, W. Nanozyme: New horizons for responsive biomedical applications. *Chem. Soc. Rev.* **2019**, *48*, 3683–3704. [[CrossRef](#)]
40. Wang, P.; Wang, T.; Hong, J.; Yan, X.; Liang, M. Nanozymes: A New Disease Imaging Strategy. *Front. Bioeng. Biotechnol.* **2020**, *8*, 15. [[CrossRef](#)]
41. Stasyuk, N.; Gayda, G.Z.; Zakalskiy, A.E.; Zakalska, O.; Serkiz, R.; Gonchar, M. Amperometric biosensors based on oxidases and PtRu nanoparticles as artificial peroxidase. *Food Chem.* **2019**, *285*, 213–220. [[CrossRef](#)]
42. Gayda, G.Z.; Demkiv, O.M.; Gurianov, Y.; Serkiz, R.Y.; Gonchar, M.V.; Nisnevitch, M. “Green” Nanozymes: Synthesis, Characterization, and Application in Amperometric (Bio)sensors. *Multidiscip. Digit. Publ. Inst. Proc.* **2020**, *60*, 58. [[CrossRef](#)]
43. Gayda, G.Z.; Demkiv, O.M.; Stasyuk, N.Y.; Serkiz, R.Y.; Lootsik, M.D.; Errachid, A.; Gonchar, M.V.; Nisnevitch, M. Metallic Nanoparticles Obtained via “Green” Synthesis as a Platform for Biosensor Construction. *Appl. Sci.* **2019**, *9*, 720. [[CrossRef](#)]
44. Stasyuk, N.; Gayda, G.Z.; Klepach, H.; Gonchar, M.V. Nanoparticles of Noble Metals as Effective Platforms for the Fabrication of Amperometric Biosensors on Hydrogen Peroxide. *Sens. Lett.* **2016**, *14*, 1169–1177. [[CrossRef](#)]
45. Liu, J.; Yang, C.; Shang, Y.; Zhang, P.; Liu, J.; Zheng, J. Preparation of a nanocomposite material consisting of cuprous oxide, polyaniline and reduced graphene oxide, and its application to the electrochemical determination of hydrogen peroxide. *Microchim. Acta* **2018**, *185*, 172. [[CrossRef](#)] [[PubMed](#)]
46. Zhao, Y.; Huo, D.; Bao, J.; Yang, M.; Chen, M.; Hou, J.; Fa, H.; Hou, C. Biosensor based on 3D graphene-supported Fe₃O₄ quantum dots as biomimetic enzyme for in situ detection of H₂O₂ released from living cells. *Sens. Actuators B Chem.* **2017**, *244*, 1037–1044. [[CrossRef](#)]
47. Niu, Q.; Bao, C.; Cao, X.; Liu, C.; Wang, H.; Lu, W. Ni–Fe PBA hollow nanocubes as efficient electrode materials for highly sensitive detection of guanine and hydrogen peroxide in human whole saliva. *Biosens. Bioelectron.* **2019**, *141*, 111445. [[CrossRef](#)] [[PubMed](#)]
48. Keihan, A.H.; Karimi, R.R.; Sajjadi, S. Wide dynamic range and ultrasensitive detection of hydrogen peroxide based on beneficial role of gold nanoparticles on the electrochemical properties of prussian blue. *J. Electroanal. Chem.* **2020**, *862*, 114001. [[CrossRef](#)]
49. Pang, H.; Zhang, Y.; Cheng, T.; Lai, W.-Y.; Huang, W. Uniform manganese hexacyanoferrate hydrate nanocubes featuring superior performance for low-cost supercapacitors and nonenzymatic electrochemical sensors. *Nanoscale* **2015**, *7*, 16012–16019. [[CrossRef](#)]
50. Zhang, C.; Zhang, Y.; Du, X.; Chen, Y.; Dong, W.; Han, B.; Chen, Q. Facile fabrication of Pt–Ag bimetallic nanoparticles decorated reduced graphene oxide for highly sensitive non-enzymatic hydrogen peroxide sensing. *Talanta* **2016**, *159*, 280–286. [[CrossRef](#)]
51. Sitnikova, N.A.; Borisova, A.V.; Komkova, M.A.; Karyakin, A.A. Superstable Advanced Hydrogen Peroxide Transducer Based on Transition Metal Hexacyanoferrates. *Anal. Chem.* **2011**, *83*, 2359–2363. [[CrossRef](#)]
52. Pandey, P.C.; Panday, D.; Pandey, A.K. Polyethylenimine mediated synthesis of copper-iron and nickel-iron hexacyanoferrate nanoparticles and their electroanalytical applications. *J. Electroanal. Chem.* **2016**, *780*, 90–102. [[CrossRef](#)]

53. Karpova, E.V.; Karyakina, E.E.; Karyakin, A.A. Communication—Assessing Stability of Oxidase-Based Biosensors via Stabilizing the Advanced H₂O₂ Transducer. *J. Electrochem. Soc.* **2017**, *164*, B3056–B3058. [[CrossRef](#)]
54. Zhou, L.; Wu, S.; Xu, H.; Zhao, Q.; Zhang, Z.; Yao, Y. Preparation of poly(N-acetylaniline)–Prussian blue hybrid composite film and its application to hydrogen peroxide sensing. *Anal. Methods* **2014**, *6*, 8003–8010. [[CrossRef](#)]
55. Karyakin, A.A.; Karyakina, E.E.; Gorton, L. Amperometric Biosensor for Glutamate Using Prussian Blue-Based “Artificial Peroxidase” as a Transducer for Hydrogen Peroxide. *Anal. Chem.* **2000**, *72*, 1720–1723. [[CrossRef](#)] [[PubMed](#)]
56. Zhang, Y.; Duan, Y.; Shao, Z.; Chen, C.; Yang, M.; Lu, G.; Xu, W.; Liao, X. Amperometric hydrogen peroxide sensor using a glassy carbon electrode modified with a nanocomposite prepared from ferumoxylol and reduced graphene oxide decorated with platinum nanoparticles. *Microchim. Acta* **2019**, *186*, 386. [[CrossRef](#)] [[PubMed](#)]
57. Karyakin, A.A.; Gitelmacher, O.V.; Karyakina, E.E. Prussian Blue-Based First-Generation Biosensor. A Sensitive Amperometric Electrode for Glucose. *Anal. Chem.* **1995**, *67*, 2419–2423. [[CrossRef](#)]